



## RESEARCH ARTICLE

10.1029/2021SW002905

### Special Section:

Space Weather Impacts on Electrically Grounded Systems at Earth's Surface

### Key Points:

- We describe the differential magnetometry method in depth and give advice on the choice of suitable instrumentation and installation site
- Uncertainty inherent in differential magnetometry is assessed, showing that noise is the main handicap; it can be minimized with filtering
- The few recent geomagnetic storm events have served to validate our model of the Spanish power network for geomagnetically induced currents assessment

### Correspondence to:

J. M. Torta,  
[jmtorta@obsebre.es](mailto:jmtorta@obsebre.es)

### Citation:

Marsal, S., Torta, J. M., Curto, J. J., Canillas-Pérez, V., Cid, O., Ibañez, M., & Marcuello, A. (2021). Validating GIC modeling in the Spanish power grid by differential magnetometry. *Space Weather*, 19, e2021SW002905. <https://doi.org/10.1029/2021SW002905>

Received 7 SEP 2021  
Accepted 12 NOV 2021



### Author Contributions:

**Conceptualization:** S. Marsal, J. M. Torta  
**Data curation:** S. Marsal, J. M. Torta  
**Formal analysis:** S. Marsal, J. M. Torta  
**Funding acquisition:** J. J. Curto  
**Investigation:** S. Marsal, J. M. Torta, O. Cid  
**Methodology:** S. Marsal, J. M. Torta, J. J. Curto  
**Project Administration:** S. Marsal, J. M. Torta

© 2021 The Authors.

This is an open access article under the terms of the [Creative Commons Attribution-NonCommercial-NoDerivs License](#), which permits use and distribution in any medium, provided the original work is properly cited, the use is non-commercial and no modifications or adaptations are made.

# Validating GIC Modeling in the Spanish Power Grid by Differential Magnetometry

S. Marsal<sup>1</sup> , J. M. Torta<sup>1</sup> , J. J. Curto<sup>1</sup> , V. Canillas-Pérez<sup>1</sup>, O. Cid<sup>1</sup>, M. Ibañez<sup>1</sup>, and A. Marcuello<sup>2</sup> 

<sup>1</sup>Observatori de l'Ebre (OE), Universitat Ramon Llull-CSIC, Roquetes, Spain, <sup>2</sup>Institut Geomodels, Departament Dinàmica de la Terra i de l'Oceà, Universitat de Barcelona, Barcelona, Spain

**Abstract** A series of experiences and recommendations are presented concerning the derivation of geomagnetically induced currents (GIC) by use of the differential magnetometry method (DMM) under power lines. This indirect technique, intended to obtain observations to validate GIC models, is an alternative to measuring the current flow in the transformer neutrals. It is a non-intrusive and autonomous technique, as the procedure does not depend on the grid operator. In contrast, the selection of suitable sites devoid of human interferences, the need for power to supply the magnetometer, the data acquisition and transmission system, along with the choice of the appropriate instrumentation are difficulties that make not just any site suitable for installation and often require costly solutions. We focus on the methodology followed to estimate the GIC flowing in several transmission lines of the Spanish power grid with the aim of validating our GIC models, and we share our experience on the installation of the measuring points. Uncertainty inherent in the DMM is assessed, showing that noise is the main handicap, although it can be minimized with appropriate filtering. According to such experience, on some occasions only total DC currents above a significant fraction of 1 A give magnetic signatures well above the noise level, so this figure can roughly be considered as the threshold limit for detection. The low solar activity, combined with the mid-latitude condition of Spain, limited the significance of available recorded data, but we can already report and analyze the results for several minor geomagnetic storms.

**Plain Language Summary** Magnetic activity within the Sun may cause intense solar storms that can affect our environment, for example by disrupting the power grids that provide our electricity. Magnetic variations primarily originated in the upper atmosphere and outer space end up inducing “slowly varying” currents in power transmission networks known as geomagnetically induced currents (GIC), which can ultimately damage power transformers and cause electrical blackouts. Resilience to this type of events depends on our progress on different fronts, one of which is the proper modeling of GIC in power grids to assess their vulnerability against magnetic storms. Once these models are operative, a fundamental step is their validation. This can be done either directly by measuring the GIC flowing in the neutral of power transformers, or indirectly by deriving the current flowing in the power transmission lines through the magnetic effect they produce. The latter has the advantage of being non-invasive for the electric utilities. We provide guidance and show our experience in this type of installations known as differential magnetometry stations, where the appropriate choice of both the instrumentation and the site is fundamental due to the main handicap of the magnitude of noise compared to the GIC signal.

## 1. Introduction

Disturbed conditions in the Sun are potential sources of events of strongly enhanced dissipation of solar wind energy in the near-Earth space environment, also known as Space Weather events, which manifest themselves as varying electric currents flowing in the coupled magnetosphere - ionosphere system. These events trigger numerous and diverse phenomena both in the surface and in the space environment of our planet. One of the consequences of such variable currents is a varying electromagnetic field on the ground that, in the presence of the conductive earth, induces an electric current in the subsurface. This, in turn, produces a secondary electromagnetic field that is superposed to the incident one, giving rise to the observed geoelectric and geomagnetic fields. Geomagnetically induced currents (GIC) are electrical currents induced in earthed conductors in response to geoelectric fields ultimately resulting from space weather events. Electric-power transmission grids and pipelines are commonly affected negatively by GIC, potentially causing problems such as damaged power transformers and

**Resources:** S. Marsal, J. M. Torta, J. J. Curto, V. Canillas-Pérez, O. Cid, M. Ibañez, A. Marcuello  
**Software:** S. Marsal, J. M. Torta, O. Cid, A. Marcuello  
**Supervision:** S. Marsal, J. M. Torta  
**Validation:** S. Marsal, J. M. Torta  
**Visualization:** S. Marsal, J. M. Torta, J. J. Curto  
**Writing – original draft:** S. Marsal, J. M. Torta  
**Writing – review & editing:** S. Marsal, J. M. Torta, J. J. Curto

increased corrosion of pipeline steel, which in turn may have an impact on key infrastructures providing services to the population such as electric power, gas or oil delivery.

Given its impact, it is not surprising that GIC modeling has become a practice of increasing interest. The geoelectric field at a given point can be estimated from the ground magnetic field and the surface impedance, which in turn is the result of the conductivity structure of the earth. The GIC flowing on earthed conductors in response to geoelectric fields depends on the power network parameters and topology, and has been established in some reference papers such as Lehtinen and Pirjola (1985) or Boteler and Pirjola (2017). Thus, a reliable model of GIC requires: (a) a consistent representation of the magnetic field throughout the area covered by the power grid, which is often related to an accurate characterization of the external sources of magnetic disturbance, (b) knowledge of the ground conductivity throughout the whole area of study, on which the geoelectric field is dependent, and (c) the network parameters such as resistances, grid topology, and the transformers and lines that are operative at the time of a given event. Assessments of the hazard of GIC in national power transmission grids have proliferated considerably in recent times (e.g., Bailey et al., 2018; Blake et al., 2018; Ingham et al., 2017; Mac Manus et al., 2017; Marshall et al., 2017). Torta et al. (2012, 2014) carried out a prediction of the effects of GIC, first on a subset and later on the entire Spanish network. GIC prediction at a transformer near the coast of the Mediterranean Sea improved significantly in Torta et al. (2017) with the inclusion of a laterally varying conductivity accounting for the sea - land interface. This result motivated a 3-D characterization of the Earth's electrical resistivity in the Iberian Peninsula by the inversion of data from magnetotelluric (MT) soundings, and the addition of the 220 kV level to the network model (Torta et al., 2021).

It follows from all the above that validation is a fundamental step in the modeling process, as it allows assessing the validity of the assumptions made in the model (i.e., earth conductivity structure, network parameters ...) by comparing its output with real GIC observations. In this paper, we show our results concerning the derivation of GIC flowing in power transmission lines by measuring their magnetic signature, which are used to validate our models. This is known as differential magnetometry method (DMM), as it uses the difference between two nearby magnetometers to compute the GIC flowing in the line. We focus on the methodology followed to achieve these results, assess the uncertainty inherent in the method, and share our experience concerning the installation of the measuring points.

## 2. Deriving the GIC

To date, the most usual way to derive the GIC is to directly capture them in the neutrals of the substation transformers. For this purpose, open-loop Hall effect transducers are generally used with an adequate data acquisition and transmission system (e.g., Torta et al., 2012). If the sampling is carried out at a sufficient rate (e.g., at 1 kHz), the recordings allow to obtain not only the direct current, but also the 50–60 Hz current present in the neutral due to the imbalances in the network or in the transformer, which is essential to determine the degree of saturation of the transformer. Temperature variations are also usually measured using thermocouples to apply the appropriate corrections in the transducers.

However, GIC can also be obtained by measuring the magnetic field they generate under the power transmission lines. This technique was developed for the derivation of GIC in gas pipelines in the 1970s (Campbell, 1978, 1980) and was applied in power lines in Finland in the 1990s (Mäkinen, 1993), more recently in Brazil (Trivedi et al., 2007), South Africa (Matandirotya et al., 2016), USA (A. Pulkkinen, personal communication), and UK (Hübert et al., 2020). Basically, it consists in performing differential magnetometric measurements by placing a vector magnetometer under a certain power line and comparing its measurements with simultaneous measurements from another magnetometer located at a distance far enough from the line to exclude the signals derived from the GIC. After processing both signals, the GIC in the power line is inferred from the difference between the measured magnetic fields using either Ampère or Biot-Savart laws. Specifically, it is the horizontal component perpendicular to the power line that is primarily used to infer the GIC. This technique has been considered as an interesting alternative for the GIC community, in contrast to the most usual means of measuring the current in the neutrals of the substation transformers, as it avoids the need to interfere with the electric utilities. However, it has been hardly used in the operational world, probably because it was not sufficiently described, or because it presents certain difficulties inherent in the indirect method of measuring currents through the magnetic

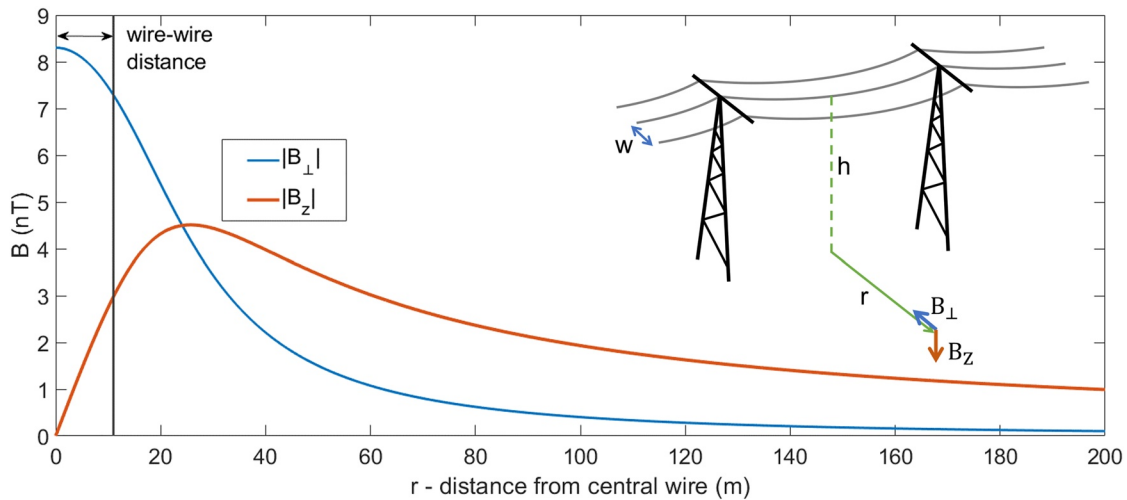


**Figure 1.** Magnetic field produced by a total geomagnetically induced current of 1 A flowing in a 3-phase power line as a function of distance,  $r$ , from the central wire. The three phase wires are assumed to have a height  $h = 20.5$  m, and a wire-wire distance of  $w = 11$  m.  $|B_{\perp}|$  (blue line) is the absolute value of the horizontal component perpendicular to the line, while  $|B_z|$  (orange line) is the absolute value of the vertical component (the parallel component,  $B_{\parallel}$ , is zero).

field they generate, which is superimposed on a series of natural and artificial signals that must be conveniently removed.

In this method, a couple of 3-axis magnetometers are placed, one below the power line, and another one typically a few hundred meters away, where the effect of the GIC is insignificant. If properly set up, the vector difference between the two magnetometers is proportional to the GIC flowing in the line.

For a correct computation of the GIC, several practical considerations must be taken into account, as shown in the following subsections. These considerations arise from the lessons learned during the installation of DMM stations aimed at quantifying the GIC flowing in several power transmission lines of the Spanish power transmission network.

### 3. Practical Considerations

#### 3.1. Selecting the Sites

First, the sites along the power line must be selected carefully, so that they are sufficiently far from artificial sources of noise, especially railways and roads. In contrast, power availability may be useful for a long-term recording to avoid battery maintenance (the latter may not be necessary for short-term DMM stations). However, in our experience, power availability is inevitably linked to the human presence, which is totally undesirable for this purpose. Fortunately, relatively affordable solutions such as solar panels can be used to supply the batteries and the equipment. On the other hand, the transmission of magnetometer data, if present, requires a good link (i.e., telephone coverage in most cases), which is not available in certain remote locations. Also, good vehicle access is desirable during installation and dismantling, as well as in the event of incidents affecting the equipment during operation, so a compromise between remoteness and accessibility must always be reached.

Once the area has been selected, we recommend the temporary (at least several hours) installation of the magnetometer under the line to ensure that the transmission line is suitable for our purposes. In our experience, it is often the case that the line carries substantial noise (of the order of 10 nanoteslas) which greatly hinders the task of estimating the GIC. If the noise level is reasonably low, the next issue to be decided is the exact location for the magnetometers. Figure 1 represents the theoretical attenuation of the magnetic components as one moves away from the power line, obtained by simple use of Ampère's law on an infinitely long straight transmission line of 20.5 m height, consisting of three wires or phases 11 m apart from each other, each carrying a DC current of 0.3 A. The attenuation of the horizontal component of the magnetic field perpendicular to the line ( $B_{\perp}$ ) is seen to be reduced to 5% of its maximum at a distance of 100 m from the line and about 1% at 200 m. Denoting  $r$



**Figure 2.** Left panel: Google Earth view of our first (pilot) differential magnetometry method station, with the mark L for mag1 and the position of the EBR geomagnetic observatory, 12 km apart. The yellow pins indicate the positions of the power line pylons. Right panel: zoom in around the location of mag1 and mag2 (the latter with the mark R) and the transmission line (in yellow). A red arrow shows the distance between the transmission line and the railway (2.4 km).

the distance (constrained to ground) from the central wire,  $B_{\perp} \sim r^{-2}$  for large distances. The vertical component ( $B_z$ ) is observed to be more persistent, as  $B_z \sim r^{-1}$  (see a more general approach to the radial dependence of the magnetic field produced by a power line, with considerations including the contribution of the induced field, in Matandirotya et al., 2016).

As noted in the introduction, it is the horizontal component of the magnetic field perpendicular to the line that is mostly used in the DMM, and this is the assumption made throughout the manuscript. In this case, it is clear from Figure 1 that the optimal location for the magnetometer near the line (hereafter mag1) is under the central wire, as it is the point with the highest  $B_{\perp}$  signal. The second magnetometer (mag2) can be placed in any suitable location where the signal goes insignificant, at least 200 m away from the line. Note that it would be possible to use  $B_z$  to infer the GIC as well; however, it is not advisable: first, because the maximum  $B_z$  signal is nearly 50% lower than that of  $B_{\perp}$  (see Figure 1); second, because  $B_z$  does not fall off as rapidly as  $B_{\perp}$ ; third, when inverting for GIC from  $B_z$  alone, the equations are more sensitive to noise.

We set our first (pilot) deployment under a transmission line that joins the substations called La Plana and Vandellòs (#69 and #132 in Figure 1 of Torta et al., 2014), mag1 was nearly under the central wire of the line, while mag2 was located in a site close to mag1, though sufficiently apart from the transmission line (320 m) to theoretically avoid its magnetic influence (see Figure 2). It is worth mentioning that we initially took Ebre observatory (EBR) headquarters, 12 km away from mag1, as the reference magnetometer (mag2). However, we observed differences of the order of a few nanoteslas between mag1 and EBR even during relatively quiet days. We have not performed a detailed study on the maximum safe distance between mag1 and mag2; instead, we refer the interested reader to Matandirotya et al. (2016), where a maximum distance of 11 km is recommended. This figure was obtained assuming a homogeneous ground conductivity; however, we note here that this value must depend on the lateral gradient of conductivity. In this sense, 11 km may be a good reference for a large province of homogeneous resistivity, but it is probably too high a value if there are nearby lateral discontinuities, particularly the land - ocean interface giving rise to the well-known “coast effect.” Therefore, based mainly on our experience, we suggest reducing this upper limit to just a few kilometers for safety.

As pointed out above, it is fundamental for the magnetometers to ensure a stable environment. Any drift caused either by varying temperature or unstable soil can mask the GIC signal. Temperature variation can be minimized by burying the instruments. The skin depth for the diurnal thermal wave is less than 10 cm for most soils, so at a depth of 20 cm the diurnal range is roughly attenuated to about 0.5–1.5°C at mid-latitudes. The resulting drift of the measured magnetic field due to the diurnal wave is acceptably low if we assume a typical temperature coefficient of 0.5 nT/°C for the magnetometer. As regards mechanical stability, it is desirable to settle the instrument on bedrock or, failing that, on a generously sized (but manageable) concrete base which can be either fixed or portable, though other solutions may exist.

### 3.2. System Requirements and Deployment

3-axis full-range fluxgate magnetometers are typically used for purposes of estimating the GIC in the DMM. The main ideal specifications for these magnetometers are:

1. Reduced temperature coefficient
2. Long-term stability of bias and scale values (the latter close to unity)
3. Linearity of the output
4. Orthogonality of the fluxgate bars
5. Low internal noise level
6. Strong attenuation of the AC signal
7. Sampling rate at least 1 Hz (filtered)
8. Low power consumption
9. Accurate time source

Some of the above features, however, are more important than others when it comes to make a cost-effective decision. In this regard, it is worth to recall that GIC timescales are roughly between 1–2 min and 3 hr (Love et al., 2018). In consequence, the magnetometer does not need to be especially stable in the long term (days and above).

Orthogonality errors should be minimized or, at least, an accurate and stable estimate should be provided by the manufacturer to correct for them during data post-processing.

The required noise level for the magnetometers can be evaluated by considering the intended resolution of the GIC signal. From Figure 1, and for the specified geometry, the magnetic signature produced by a DC current of 1 A under the line is seen to be about 8 nT. According to our experience, typical values range between 8 and 20 nT/A. GIC signals use to be significant above 1 A, so a resolution better than 0.1 A is seldom needed, which typically translates into 0.8–2 nT for the difference between the magnetic components measured by the two magnetometers assuming they are perfectly aligned. Further assuming that the uncertainty in the difference propagates in quadrature, the maximum noise allowed in the GIC frequency band for a single magnetometer is 0.6–1.4 nT, for which 1 nT can be taken as an average reference figure.

For the magnetometer operating under the line, the AC signal can be at least two orders of magnitude higher than that of the maximum expected GIC, so it requires an effective attenuation in the 50–60 Hz band by appropriate built-in filtering.

Minimal temperature drift is critical if constant temperature cannot be guaranteed. However, the impact of changing temperature can be minimized by digitally filtering periods above the maximum expected period of GIC (~3 hr). For conditions easily achievable in the field being combined with appropriate filtering, a temperature coefficient for the fluxgate bars of 1 nT/°C is generally sufficient. Further digital filtering of short periods below 1 or even 2 min corresponding to the fastest GIC periods is a common practice to avoid noise. We use simple Gaussian filters for these purposes.

Low power consumption is especially important for remote sites, often powered by unattended batteries, whether or not fed by solar panels. In our first deployment (Figure 2), power supply was available from a nearby farm, allowing a battery charger to keep the batteries at an appropriate level, thus avoiding a frequent replacement.

While the above specifications are minimum requisites, it is also desirable to count on a transmission system to ensure data retrieval beyond local storage. Besides, this equipment allows continuous control and an immediate diagnosis of possible problems affecting the remote deployments, thus avoiding data loss. We have deployed a low-cost, low-consumption data-transmission system using a Raspberry Single Board Computer (SBC) with a General Packet Radio Service (GPRS) shield to transmit the magnetometer data to Ebre Observatory headquarters once a day.

Following our first experience with inadequate instrumentation at the locations described in Section 3.1, a set of LEMI 44 magnetometers meeting the specifications outlined above was purchased, two of which were initially settled replacing the previous ones at the same location. The rest have been or will be deployed in other temporary DMM stations along different power lines across the Spanish power grid to assess GIC in sites identified

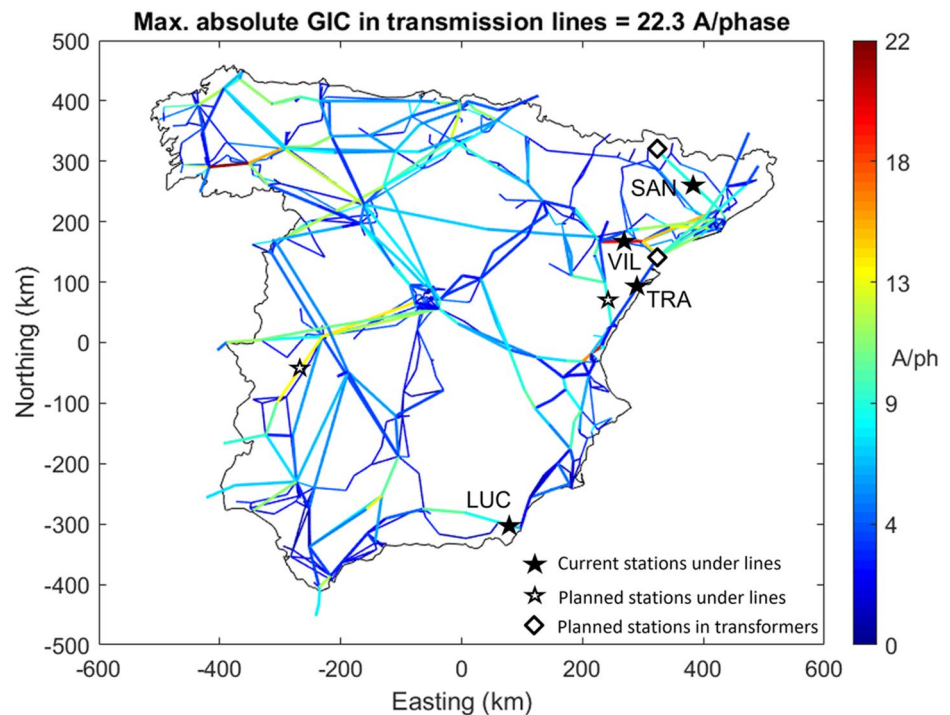


**Figure 3.** Map of mainland Spain showing the maximum absolute geomagnetically induced currents (A/phase) along the power lines that would have been recorded during the Halloween storm with the present power grid. The most vulnerable lines are shown in warm colors. Thin lines represent 220 kV lines, while thick ones correspond to 400 kV lines. Symbols indicate current and newly planned differential magnetometry method stations. The three-letter codes assigned correspond to the initial letters of the municipality where each station is located.

as hazardous due to the network topology and resistances, or where the power grid model, together with the estimated surface impedance, must be validated. Current and newly planned DMM stations according to these conveniences are indicated in Figure 3.

Each magnetometer is placed inside a water-proof PVC container that is buried to attenuate the thermal oscillation. For correct leveling and orientation, a base with specially manufactured leveling foot screws attached with PVC cylinders accessible from the top is included (Figure 4).

Despite the logistic advantages provided by the site chosen for our pilot experience, the DMM station proved to be excessively noisy due to the proximity of an urban center, roads and a railroad. For this reason, a new, more isolated site was chosen under the same power line, 30 km further SW, in the municipality of Traiguera (TRA). A pair of magnetometers were installed there in December 2019 in the manner described above, but the Mediterranean storm Gloria, which hit eastern Spain and southernmost France with strong winds and heavy rainfall on 19 January 2020 flooded the field and caused water to enter the electronic devices, rendering them inoperative until repaired quite a few months later. After that bad experience, external connections (i.e., those necessary to power both the magnetometer and the transmission module, to connect a GPS antenna and to take out an antenna for data transmission) were made through an appropriate siphon bend pipe with bushing wall isolators (Figure 4). In addition, all external cabling was protected against rodents by placing it inside tough polyethylene irrigation tubing.

The same operation was repeated in Sanaija (SAN), Lucainena (LUC), and later on, in Vilalba (VIL). However, new difficulties arose, such as condensation water dripping from the lid of the PVC container into the magnetometer through its Secure Digital (SD) card slot, leading to further electronic failures and long interruptions in the service. We also observed that the placement of the transmission modules on top of the magnetometers (as in Figure 4) caused excessive noise that rendered many records unusable until we placed them a few meters away. After so much trial and error in designing the optimum installation, we have finally come up with a suitable piece of equipment, but in the meantime, this has meant that the availability of usable data is still limited. Fortunately,



**Figure 4.** Top: Lemi 44 magnetometer (left) and its bespoke PVC water-proof container (right), which, for the proper leveling and orientation, includes a concrete base to provide stability with leveling foot screws attached with PVC cylinders accessible from the top. Bottom: The magnetometer placed inside its container is buried to attenuate the thermal oscillation. The electronic box on the top contains the data transmission module.

geomagnetic activity over the last year has been very low coinciding with the minimum of the solar cycle and the first significant storm has not occurred until 12 May 2021, with all four DMM stations fully operational (see Figure 5).

### 3.3. Magnetometer Orientation

Figure 1 shows that, although the vertical component of the magnetic field is nil under the central wire, it takes a significant value below the peripheral ones. This fact suggests that the magnetometer under the power line must be well oriented, with two sensor axes in the horizontal plane and the other pointing vertically to avoid contamination between components. There are, however, different but equally valid orientations in the horizontal plane. One possible orientation is one axis parallel to the line and the other perpendicular to it. This option benefits from the fact that the latter axis directly records the magnetic signal of the GIC in the case of mag1, while the parallel axis only records the natural geomagnetic variation. However, the orientation of mag2 according to this frame is not straightforward in the field (note that it is preferable that both magnetometers have the same orientation). Another (more suitable) option is orienting both magnetometers according to the local magnetic field, that is, one axis pointing magnetic north, another pointing magnetic east and the third pointing vertically downward. This orientation is easily attainable for both instruments, as the operation simply consists in searching for a null output in the appropriate magnetometer channel by rotation in the horizontal plane, while keeping the third channel vertically aligned. This option has the additional advantage that the magnetograms are directly comparable to nearby observatory data (assuming the Declination angle is sufficiently small), thus allowing a preliminary check of the whole data set. The magnetic signal of the GIC (i.e., the component perpendicular to the line) is simply obtained by applying a virtual rotation on the data during the post-processing, as will be shown later.

Figure 6 shows the differences on the horizontal components recorded by mag1 and mag2 (i.e.,  $X_1 - X_2$ ;  $Y_1 - Y_2$ ) at TRA during the most disturbed day since the station was settled. The relatively small differences observed at the times of highest disturbance are due to the GIC flowing along the power line.

### 3.4. GIC Computation

The raw data obtained by DMM stations require post-processing to determine the GIC. Let  $\vec{B}_1^0(t) = (X_1^0(t), Y_1^0(t), Z_1^0(t))$  be the output of mag1 magnetometer under the line, with  $X, Y, Z$  denoting the (arbitrarily oriented) vector components, and  $\vec{B}_2^0(t) = (X_2^0(t), Y_2^0(t), Z_2^0(t))$  the output of mag2.

In general, a series of corrections must be applied to the components of each

magnetometer based on the manufacturer specifications, namely: scale factor, bias and orthogonality errors, which can be summarized as

$$\begin{pmatrix} X_i \\ Y_i \\ Z_i \end{pmatrix} = \begin{pmatrix} k_{X,i}^0 & -\varepsilon_{xy,i} & 0 \\ 0 & k_{Y,i}^0 & 0 \\ -\varepsilon_{xz,i} & -\varepsilon_{yz,i} & k_{Z,i}^0 \end{pmatrix} \begin{pmatrix} X_i^0 \\ Y_i^0 \\ Z_i^0 \end{pmatrix} + \begin{pmatrix} b_{X,i}^0 \\ b_{Y,i}^0 \\ b_{Z,i}^0 \end{pmatrix} \quad (1)$$

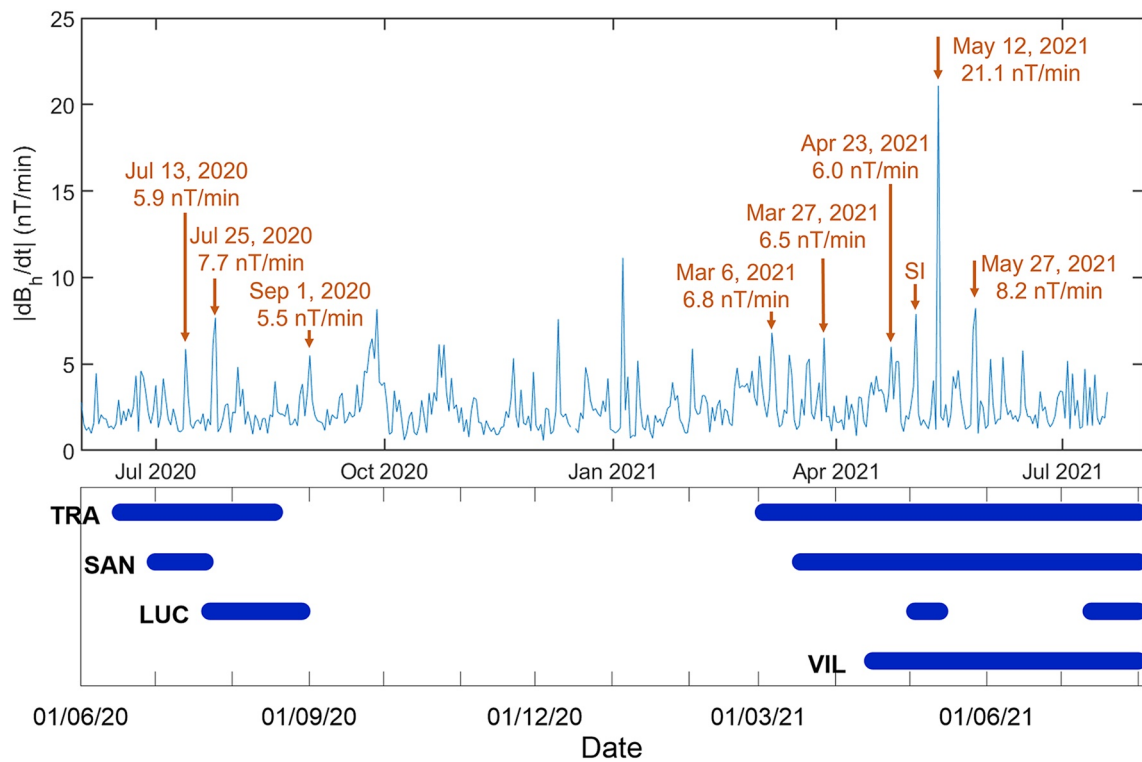


**Figure 5.** Geomagnetic activity at EBR observatory given by the maximum amplitude of the time derivative of the horizontal magnetic field vector for each day (top). Labeled data tips at the top panel indicate days with data availability at any of the differential magnetometry method stations (bottom) when  $|d\vec{B}_h/dt|$  was equal to or greater than 5.5 nT/min (except when corresponding to an isolated sudden impulse, SI).

where  $i = 1, 2$  stands for mag1 and mag2, respectively;  $\vec{B}_i = (X_i, Y_i, Z_i)$  are the corrected values;  $k_{X(YZ),i}^0$  is the X(YZ)-sensor scale value, assumed to be unit-less and close to unity;  $\varepsilon_{jk,i}$ , in radians, are small orthogonality errors, defined in such a way that  $\pi/2 - \varepsilon_{jk,i}$  is the angle between the component sensors  $j$  and  $k$  relative to

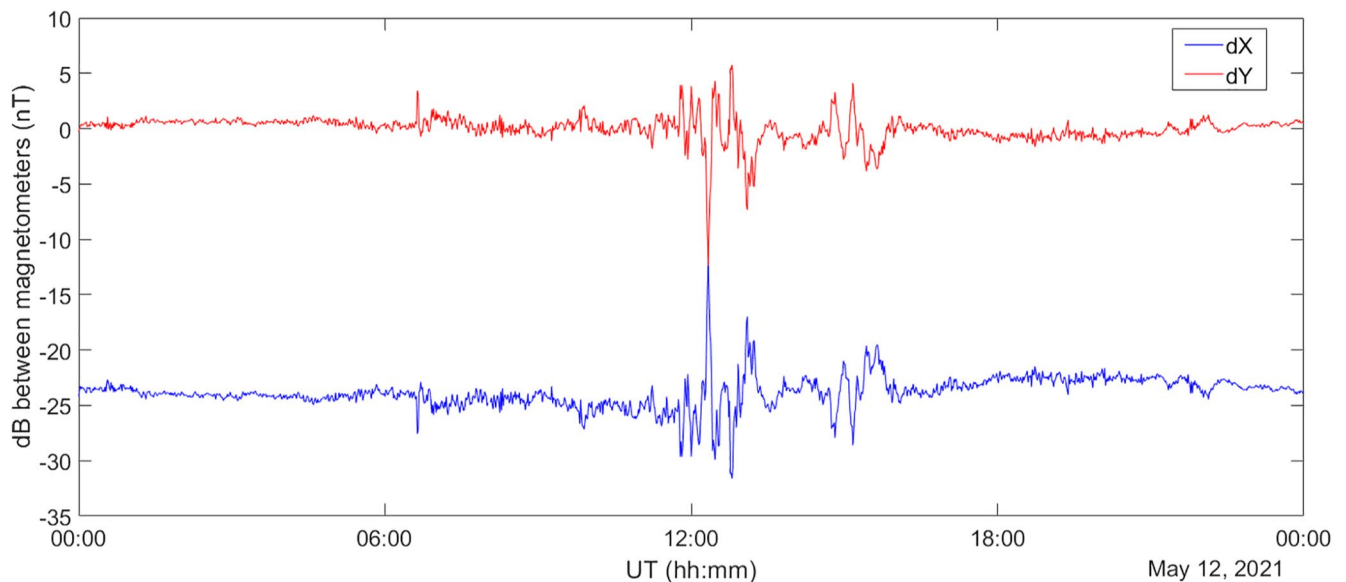


**Figure 6.** Differences between the magnetic horizontal components below the transmission line and at the reference location during 12 May 2021, as recorded at TRA differential magnetometry method station. Blue and red lines correspond to X (north in this case) and Y (east) channels, respectively.



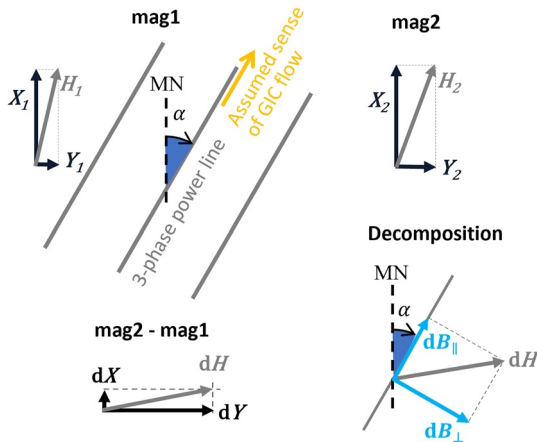


**Figure 7.** Schematic showing the two magnetometers of a DMM site from above. The upper left panel (labeled mag1) shows mag1 orientation, with its X axis pointing magnetic north (MN) in this case, making an angle  $\alpha$  with the transmission line. The orientation of mag2, in the upper right panel, is parallel to mag1. The lower left panel shows the vector difference between mag2 and mag1 (note that mag1 may have undergone a small rotation, according to Equation 2). The lower right panel shows the decomposition of the vector difference along the line and transverse to it.

magnetometer  $i$ ; and  $b_{X(YZ),i}^0$ , in nT, is the bias of the X(YZ) sensor, which is assumed to be much smaller than the total field  $F$ .

Note that, in general, the corrected vectors for mag1 and mag2 are given in different reference frames. This is generally true although efforts are carried out to properly orient the magnetometers, as conditions in the field are rarely ideal. In consequence, in a subsequent step it is advisable to find the rotation that passes from the frame of mag1 to the frame of mag2. This can be achieved by minimizing the vector

$$\begin{pmatrix} dX \\ dY \\ dZ \end{pmatrix} = \begin{pmatrix} X_2 \\ Y_2 \\ Z_2 \end{pmatrix} - \mathbf{R}(\varphi, \theta, \psi) \begin{pmatrix} X_1 \\ Y_1 \\ Z_1 \end{pmatrix} \quad (2)$$

in the least-squares sense. The matrix  $\mathbf{R}$  in Equation 2 represents the mentioned rotation, which in general depends on the angles  $\varphi$ ,  $\theta$  and  $\psi$ . Note that expression (2) in reality has 3 unknowns (the rotation angles) and  $3n$  equations, where  $n$  is the number of time samples being considered, for example,  $n = 1,440$  for a daily file of 1-min values. The residuals, i.e., the left-hand side of Equation 2, is the part that the rotation cannot account for, and can be interpreted as the magnetic signature of the GIC expressed in the frame of mag2. Prior to the application of the least squares, it is always advisable to perform a virtual rotation of mag2 around its Z axis, so that the mean value of the Y component is suppressed (we are assuming here that the local magnetic

frame is sought). This operation results in the X axis of mag2 close to the magnetic meridian. An alternative to the least-squares procedure is to perform a virtual rotation of both magnetometers around their Z axes as explained above, so that the X axes of the two magnetometers are set close to the magnetic meridian. After that, a second rotation around the Y axis (i.e., in the XZ plane) of mag1 is performed so that its average magnetic inclination coincides with that of mag2. The latter procedure is accurate enough as long as the leveling of the two magnetometers do not differ significantly (a few degrees allowance), which is normally accomplished to a sufficiently good approximation even under conditions in the field. The least-squares technique, on the contrary, would allow for an arbitrary orientation of mag1, that is, not necessarily level or oriented according to the local magnetic field, as the optimal rotation would take care of getting it to the right orientation (that of mag2, which does need to be at least as level as possible).

Note that any of the two procedures described above to match the frames of the magnetometers has the shortcoming that the GIC signal itself disturbs the magnetic field of mag1, especially when the magnitude of the event is considerable, thus distorting the true values of the rotation angles. This difficulty can be circumvented by determining these angles based on a significant number of quiet days around the disturbed day of interest, and apply them on that disturbed day, thus allowing no parameters to be adjusted during the event.

Let us now assume that, after the above rotations, the Z axes of the magnetometers nearly point vertically downwards. A new rotation in the horizontal plane will translate the residual vector into the reference frame of the transmission line. This is achieved by the following operation

$$\begin{pmatrix} dB_{\parallel} \\ dB_{\perp} \end{pmatrix} = \begin{pmatrix} \cos \alpha & \sin \alpha \\ -\sin \alpha & \cos \alpha \end{pmatrix} \begin{pmatrix} dX \\ dY \end{pmatrix}, \quad (3)$$

where  $\alpha$  is the angle that the X axis of mag2 needs to be rotated (positive clockwise) to point in the desired sense of positive current flow on the transmission line. Thus, the chosen value for  $\alpha$  (given the ambiguity of  $180^\circ$ ) determines the sense in which the GIC is considered positive; equivalently,  $\alpha + 180^\circ$  would define the opposite sense of GIC flow. Figure 7 shows a representation of the above for an X axis of both magnetometers pointing magnetic north. Note that the assumed sense of positive GIC flow in the figure is north-east for  $\alpha \sim 30^\circ$ , while it would be south-west if a value of  $\alpha \sim 30^\circ + 180^\circ = 210^\circ$  had been chosen.

The angle  $\alpha$  thus depends on the chosen frame for the magnetometers. It is zero for an X axis parallel to the line, and equals the magnetic azimuth of the power line for an X axis pointing magnetic north. An approximate value for  $\alpha$  in this latter case can be obtained by subtracting the local declination (which in turn can be obtained either by use of a DIflux theodolite, taking the value from the nearest observatory, or even using online calculators, for example, <https://www.ngdc.noaa.gov/geomag/calculators/magcalc.shtml>) from the true north orientation of the line provided, for example, by Google Earth.

The magnitude of interest in Equation 3 is  $dB_{\perp}$ , as it is the computed magnetic signal of the GIC. However, the value of  $dB_{\parallel}$  may serve to quantify the error of our GIC estimation, as its value is theoretically zero.

As mentioned above, the GIC is proportional to  $dB_{\perp}$  in the form  $GIC = dB_{\perp}/s$ , where the proportionality constant,  $s$ , must be determined in terms of the geometry of the transmission line and the location of mag1. In particular, one has to make use of Ampère's law to calculate the horizontal component of the magnetic signal produced by a unitary (i.e., 1 A) total current flowing through the three wires of the transmission line, on the location of mag1 (see Figure 1). The calculation thus depends on the relative position of the line and the sensor, and the particular geometry of the wires making up the line, i.e.,  $h$ ,  $r$  and  $w$  parameters. In our first pilot experience, the three wires are laid at the same height at the location of the power line where we deployed the magnetometer, but there exist other pylon geometries, so that the different heights of each wire should be taken into account (Hübert et al., 2020); also, pylons can support multiple power lines, and the GIC flowing in each of them, of course, generates magnetic fields that are measured altogether by the magnetometer. As mentioned above, typical values for  $s$  found by us range between 8 and 20 nT/A.

#### 4. Assessing the Uncertainty Associated With the DMM

In this section we provide an estimate of the uncertainty associated with the indirect measurement of the GIC with the DMM. We apply error propagation from the main sources of uncertainty throughout the chain of steps implied by the experiment. Even if this exercise was carried out by Hübert et al. (2020), we present here our independent estimate based on our own experience. An analysis of the uncertainties reveals the following sources of error:

1. The uncertainty of the magnetic field provided by the magnetometers measuring the effect of the GIC depends on several factors: (a) the power spectrum of the instrument internal noise. This is a function of frequency, for which we know that the value for the LEMI 44 at 1 Hz is around  $0.05 \text{ nT}\cdot\text{Hz}^{-1/2}$ . A discussion on the frequency dependence of the power spectrum is provided by Korepanov et al. (2001). The function is to be integrated among the minimum and maximum frequencies being measured, for which we use the boundary frequencies of our digital band-pass filter between 2 min ( $8.3\cdot 10^{-3}$  Hz) and 5 hr ( $5.6\cdot 10^{-5}$  Hz), providing a total noise level of 0.11 nT. Note that the GIC depends on the difference between two magnetometers, so the noise propagates as  $(0.11^2 + 0.11^2)^{1/2} = 0.16 \text{ nT}$  if we assume that both magnetometers have an equivalent performance; (b) the uncertainty associated with the scale factors ( $k_j^0$ ) and orthogonality errors ( $\varepsilon_{jk}$ ), for which we use the manufacturer values. These uncertainties are stated to be around 0.02% and  $3.5\cdot 10^{-4}$  rad, respectively. The combined uncertainty is thus about 0.04%. Note that the latter is a relative error that scales with the magnetic field and thus with the GIC, rendering it negligible for all practical purposes.
2. The influence of the magnetometer misalignment with respect to an ideal geomagnetic reference frame (perfect leveling and X and Y axes pointing, for example, magnetic north and east, respectively) is evaluated here. LEMI 44 instruments incorporate a circular level that allows leveling the instrument with a precision of typically  $0.3^\circ$ . A tilt of this size produces a penetration of the vertical variations as large as  $\Delta Z \sin(0.3^\circ)$  in the horizontal components. During disturbed times, which are precisely the most interesting for GIC evaluation,  $\Delta Z$  may be of the order of tens or even hundreds of nanoteslas. A plausible value of 70 nT at midlatitudes gives a 0.4 nT spurious component in the horizontal field. The same argument can be applied to rotations in the horizontal plane, though the spurious component can be somewhat higher in this case, as the horizontal variations are typically greater than the vertical ones. We assume that the combination of the horizontal and vertical spurious components due to misalignment between mag1 and mag2 is of the order of 1 nT during moderately disturbed conditions. However, the estimated GIC depends again on the difference between mag1 and mag2. If both magnetometers had exactly the same orientation, even if not the ideal one, the mentioned spurious component would cancel out. The virtual rotation of the frame of mag1 to meet the frame of mag2

(Equation 2, Section 3.4) is intended for this cancellation. However, tests show that the effectiveness of those rotations to cancel the spurious components are limited in practice, and residual variations of 0.5–0.6 nT are seen to persist.

3. It is usually assumed that the reference magnetometer is far enough away from the power line so that it does not pick up its magnetic influence. Placing it at 200 m (150 m), however, the horizontal component  $B_{\perp}$  can be evaluated to be about 1% (2%) of its value under the line (see Figure 1). This is equivalent to reducing the geometric factor  $s$ , and thus increasing the final value of the GIC, by this amount. On the other hand, because the vertical component of the magnetic field produced by the line ( $B_z$  in Figure 1) attenuates slowly with distance, it can have a non-negligible influence on mag2 if both magnetometers are at a different altitude, even if they are perfectly oriented. In one of our deployments, mag2 is located  $14^{\circ}$  below the horizon as seen from the power line, 180 m downhill from it. Taking  $B_z = 1.1$  nT/A for  $r = 180$  m from Figure 1, the horizontal projection of the magnetic field produced by the line at the location of mag2 is  $1.1 \cdot \sin(14^{\circ}) = 0.27$  nT/A, which is 3% the value of  $B_{\perp}$  under the line. Note that this reduces the effective value of  $s$  in this case, but would increase it if the altitude of mag2 were higher than that of the line. Finally, it has been argued that mag2 should not be placed so far away from mag1 that the measured natural magnetic variations are different in both sites. Placing mag2 at a distance of less than 5 km from mag1 should not produce differences in such variations of more than 0.1 nT.
4. Temperature variations and instrument motions have a negative impact on the accuracy of the measured magnetic field. As stated above, typical diurnal variations for buried instruments range in the order of  $1^{\circ}\text{C}$ , implying a wave with an amplitude of 0.5 nT for a typical drift of the fluxgate components of  $0.5$  nT/ $^{\circ}\text{C}$ . Using a cutoff frequency for our band-pass filter of  $5.6 \cdot 10^{-5}$  Hz (5 hr period) in the lower boundary, this implies an attenuation of ca. 37 dB for the diurnal variation, rendering a negligible signal around 0.01 nT. We refer to motions as transient movements of the magnetometers. Evaluating their magnitude for a buried instrument within a typical period of 5 hr is beyond our capabilities, as it depends on many factors such as changing soil conditions and soil permeability. A plausible value of a few arc-seconds during this time window would be possible after heavy rainfall or during the first days after instrument deployment in the field, in which case the associated variations could be well above the aforementioned noise threshold of 0.11 nT. A significant drift is in fact observed after the first few days of installation.
5. The impact of the geometric factor  $s$  is evaluated here. For the configuration shown in Figure 1 (one transmission line with the three wires at the same height), the formula for  $s = B_{\perp}/\text{GIC}$  is obtained with Biot-Savart law.

$$s = \frac{\mu_0 h}{2\pi} \frac{1}{3} \left( \frac{1}{h^2 + r^2} + \frac{1}{h^2 + (r - w)^2} + \frac{1}{h^2 + (r + w)^2} \right). \quad (4)$$

This function has a maximum at  $r = 0$  ( $r$  is the distance from the ground projection of the central wire), so moving mag1 within 2 m from the exact location underneath the central wire has minor consequences for the estimated GIC (typically less than 0.5% relative error).  $h$  (the height of the wires) can be estimated in different ways: with a laser range meter the uncertainty, in our experience, is in the centimeter range. However, the depth of the fluxgate sensor must be added to the previous estimate. Additional errors arising from the biased pointing of the laser in a plane not perpendicular to the power line could result in an overall uncertainty of 0.15 m. This propagates into  $s$  in an amount of less than 1%. A theodolite has also been used to determine  $h$ , with a vertical measuring rod 4 m long being used as a reference below the wires. The uncertainty is typically larger in this case, as the terrain is irregular and the difference in elevation of the base of the rod and the buried magnetometer sensor is difficult to evaluate, among other sources of uncertainty. 0.5 m is a reasonable bound for the uncertainty of  $h$  in this case, leading to a 3% uncertainty in  $s$ .  $w$  (the wire-wire distance) is estimated by measuring the angular distance of the wires in the neighboring pylon(s) by use of a theodolite. This procedure requires knowledge of the theodolite - pylon distance, which can be precisely determined with Google Earth, thus providing an uncertainty for  $w$  that does not exceed 0.2 m. The latter translates into  $s$  by  $\sim 0.5\%$  uncertainty. The largest uncertainty in  $s$  is thus associated with the uncertainty of  $h$ . Because  $s^{-1}$  is a factor multiplying the differential magnetic field, we can conclude that the relative uncertainty of the estimated GIC due to the geometry is roughly 1% if we use a laser range meter, or 3% if we use a theodolite. Note that the discussion

above is focused on our first deployment (Figure 1); however, tests with the other pylon configurations and geometries that we have found in our deployments provide very similar results.

6. The procedure to estimate the GIC goes through the value of  $\alpha$  (Equation 3), the angle between the X axis of the magnetometers and the power line. Rotating the reference frame by this angle minimizes  $dB_{\parallel}$  and maximizes  $dB_{\perp}$ , reason by which an accurate value is not critical. Let us estimate, however, the associated uncertainty. Assuming that the magnetometers are oriented according to the local magnetic field, which is the most reasonable choice, we can write  $\alpha$  as  $Az - D + \delta$ , with  $Az$  the azimuth of the power line with respect to true north,  $D$  the magnetic declination at the DMM site, and  $\delta$  the misalignment of mag1's east component ( $Y_1$ ) with respect to magnetic east. Using Google Earth provides a high accuracy ( $\sim 0.1^\circ$ ) for  $Az$ . On the other hand, using the nearest geomagnetic observatory for the epoch of interest provides a reasonable estimate for  $D$ , though online calculators may also be used, both methods providing accuracies below  $0.1^\circ$ . The largest uncertainty is associated with the true orientation of mag1 in the field. A mean value of the magnetometer's east component ( $Y_1$ ) allows to calculate  $\delta$ ; however, this estimate is subject to the perfect leveling of the instrument, which is not feasible in the field beyond typically  $0.3^\circ$ . For our midlatitude sites, with a magnetic inclination of  $56^\circ$ , this implies an error of  $0.3^\circ \cdot \tan(56^\circ) \sim 0.4^\circ$  in the true orientation of the magnetometer.  $dB_{\perp}$  (and thus the estimated GIC) is entirely insensitive to an error of  $0.4^\circ$  (or even more) in  $\alpha$ .
7. Ambient noise, whereas it is extrinsic to the measurement process itself, can significantly mask the true value of the GIC. We have found different types of noise in our deployments. White noise recorded in our 1-s data is effectively reduced with our digital filter by about a factor of eight. For a maximum white noise component of ca. 10 nT, this gives a residual noise of the order of 1 nT. Other components of the noise include sporadic spikes and a variety of transient phenomena lasting for an indefinite time which are not effectively removed by the filter. Although de-spiking is included in the pre-processing of the data, the above variations give rise to false GIC signals which, in some DMM deployments, can reach several nanoteslas or, when translated to GIC, a significant fraction of an amp. We have no experience evaluating the noise introduced by peripheral devices (e.g., cabling and transmission system), though a test in the field could be carried out by temporarily disconnecting some components or using shorter cables.

Assuming that the uncertainties propagate in quadrature, only the highest values prevail. Combining the internal noise and the errors arising from imperfect leveling/orientation of the magnetometers yields an upper limit of 0.6 nT absolute uncertainty. This typically translates into 0.06 A or less for the calculated GIC, which is negligible in terms of impact on the power network and suitable for our purposes to validate the GIC modeling in the Spanish power grid. As for relative errors, combining the uncertainty derived from the determination of  $s$  and that of the finite distance between mag2 and the power line (among other minor errors) gives an upper limit of 1.5% uncertainty in the GIC, which is excellent for most purposes. The latter assumes that a laser range meter is used to measure the height of power lines; if a theodolite is used instead, 3% is a more appropriate figure. In these final values we also assume that the data are band-pass filtered and that virtual rotations are performed on the magnetometer frames so that their variations can be subtracted consistently; otherwise, the error is highly dependent on the accuracy of the initial leveling and orientation. Finally, note that the above figures apply to our particular magnetometers and procedures, and are not necessarily applicable to others. In this context, we conclude that our instrumentation is well suited for accurate estimation of the GIC flowing in the power grid, the main limitation being imposed by the ambient noise, which in most cases flows in the power line itself. The time evolution of the quantity  $GIC_{\parallel} = dB_{\parallel} / s$ , which can be obtained from Equation 3, provides an independent, rough estimate of the uncertainty associated with the GIC, as its value is theoretically zero.

## 5. Results

Figure 8 shows a comparison of the computed and modeled GIC again at TRA during 12 May 2021. The former is obtained with Equations 1 and 2 by use of least squares. The modeled GIC is obtained by using the geomagnetic field measured at the Spanish and surrounding observatories and the network and earth resistivity models described in Torta et al. (2021). To date, this is the most disturbed day since the station was settled. As mentioned above, a band-pass filter has been applied to both sets, so as to cut periods below 2 min (to smooth high-frequency undesired signals) and above about 5 hr (thus avoiding drifts or temperature effects on the magnetometers). Note that this site is comparatively clean of ambient noise.

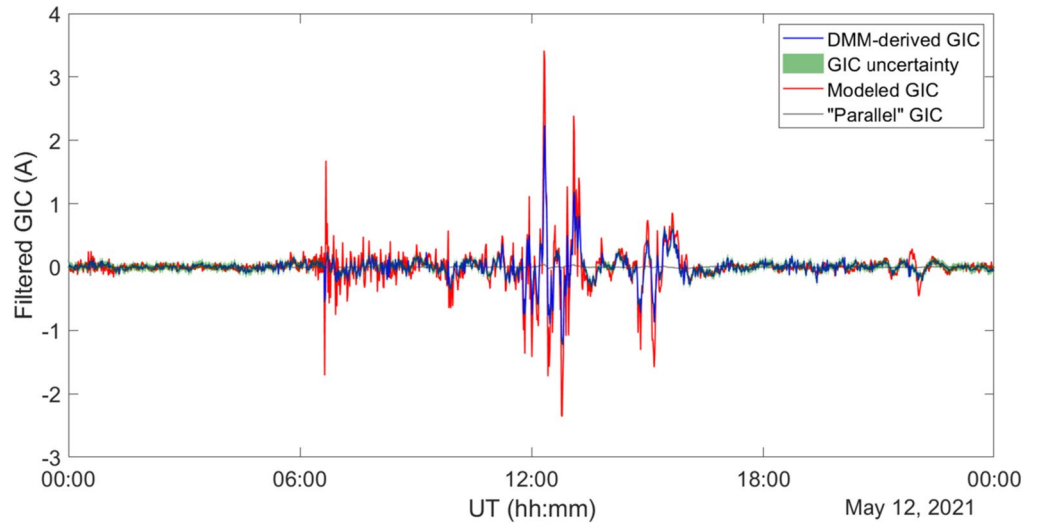


**Figure 8.** Modeled (red line) versus differential magnetometry method-derived (blue line) geomagnetically induced currents (GIC) flowing on 12 May 2021 through the power line where TRA DMM station is located. The narrow green envelope around the derived GIC represents its intrinsic uncertainty, while “parallel” GIC (gray line) represents the obtained current component parallel to the power line ( $GIC_{\parallel}$ ).

To evaluate the agreement between the DMM-derived and modeled GIC, a combination of the linear correlation coefficient,  $\rho$ , and the performance parameter,  $P'$ , between both time series has been used (see Marsal & Torta, 2019).  $P'$  is defined as

$$P' = 1 - \frac{\sigma_{o-m}}{\sigma_o}, \quad (5)$$

where  $\sigma_o$  is the standard deviation of the observation series (i.e., the GIC derived following the exposed methodology), and  $\sigma_{o-m}$  is the standard deviation of the differences between the observations and the model. Note that a perfect match between model and data would give  $P'$  and  $\rho$  equal to unity; in the extremely opposite case, these parameters can be as unfavorable as minus infinity and 0 (note that  $\rho < 0$  would denote a negative correlation, indeed), respectively. Table 1 is set to provide these skill scores during the events indicated in Figure 5 at each DMM station with available data. Events have been selected including only those with maximum  $|d\vec{B}_h/dt|$  values equal to or greater than 5.5 nT/min, except for that of 3 May 2021, which corresponded to an isolated sudden

**Table 1**  
*Linear Correlation Coefficient ( $\rho$ ) and Performance Parameter ( $P'$ ) to Evaluate the Agreement Between Differential Magnetometry Method (DMM)-Derived and Modeled GIC at the DMM Stations With Available Data During the Events Indicated in Figure 5*

Event	TRA		SAN		LUC		VIL	
	$\rho$	$P'$	$\rho$	$P'$	$\rho$	$P'$	$\rho$	$P'$
13–14 July 2020	0.50	−0.29	0.61	−0.25				
24–25 July 2020	0.67	−0.30			0.96	0.69		
28 August 2020 to 01 September 2020					0.97	0.70		
06–07 March 2021	0.67	−0.12						
24–28 March 2021	0.65	−0.03	0.60	−0.11				
23–26 April 2021	0.61	−0.15	Power line switched off				0.59	−0.58
12 May 2021	0.88	0.08	0.82	0.05	0.96	0.71	0.73	−1.83
26–27 May 2021	0.70	−0.03	0.74	0.06			0.66	−0.98

*Note.* The duration of each event was selected to include whole days with a certain magnetic activity. It was sufficient that the rate of change exceeded 5.5 nT/min during one of the days of the event for it to be selected. Blank cells denote unavailable data.

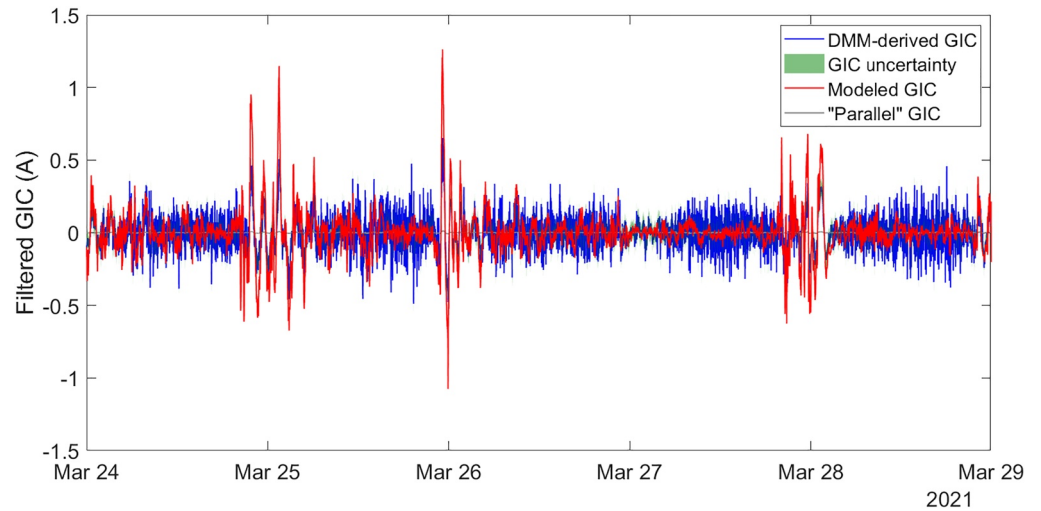


**Figure 9.** Modeled (red line) versus differential magnetometry method (DMM)-derived (blue line) geomagnetically induced currents (GIC) flowing on 24–28 March 2021 through the power line where SAN DMM station is located. The green envelope (hardly visible in the figure) around the derived GIC represents its intrinsic uncertainty, while “parallel” GIC (gray line) represents the obtained current component parallel to the power line ( $GIC_{\parallel}$ ). The latter is clearly lower than the estimated GIC, denoting that the line carries the noise. The DMM-derived GIC is clearly noisy during day hours compared to night hours.

impulse (SI) with the rest of the day being very quiet. Although the effect of the GIC was indeed measured by our differential set of magnetometers, that event has been excluded from the table because the correlation with the modeled GIC during the whole day was very poor, as the noise prevailed over the signal.

In general, values for both skill scores tend to improve with geomagnetic activity, reflecting the increase in signal-to-noise ratio. Except in the case of LUC, negative or close to zero values of  $P'$  reveal poor matches as a consequence of model overestimation (as is the case for TRA, according to the example of Figure 8) or underestimation (as is the case for LUC, according to Figure 11 of Torta et al., 2021) of the computed signal. These discrepancies are mainly due to the numerous assumptions made concerning the resistances of the network elements but also to having ignored circuits with voltage levels below 220 kV in the power grid model. Indeed, there are 110 kV power lines galvanically connected through autotransformers in the substations at both ends of the power line passing through VIL, and at one end of the lines passing through TRA and SAN. However, the two ends of the power line passing through LUC are only connected to 400 or 220 kV power lines, all of which are included in the power grid model. This could be the reason why we have obtained such a high score for  $P'$  there. Note that a perfect matching is practically unreachable (Marsal & Torta, 2019), since  $P'$  rarely exceeds 0.6–0.7 (e.g., Torta et al., 2017) even for good GIC models.

Except for LUC station, another reason for the mismatches shown in several of the events in Table 1 is the fact that on those occasions the records in the magnetometers located under the power lines show numerous spikes, and even jumps, being in general more numerous and of greater magnitude during day hours. On the contrary, the records on the reference magnetometers are always clean. This incidents were already reported by Matandirotya et al. (2016), and we, like them, believe that they are related to power grid switching or voltage transients originating from high-power-demanding on the end load of power transmission and distribution networks, which result in changes in power line currents, whose magnetic effects are not effectively filtered in the one-second data provided by the magnetometers. Schachinger et al. (2021) have recently reported that they have measured and identified sources of low frequency currents by measuring GIC in several power transformer neutrals in Austria originating from DC powered public transportation leakage currents that would enter the transmission system. In general, our spikes are sporadic at night hours and can be manually cleaned up when data are being processed, but during the day, they produce noisy magnetic records that could mask GIC signals if they are tiny enough. An example of a noisy DMM-derived GIC signal is shown in Figure 9. Notice that the signal is much cleaner around midnights. The type of noise at this station (SAN) is white and on the order of 10 nT during daytime, reducing to 1.3 nT after filtering. This results in a noise with a semi-amplitude about 0.1 A in the GIC signal.

An additional circumstance that has affected our records during the period April–June 2021 has been a series of forced or unforced outages at the Ascó and Vandellòs nuclear power plants, which connect directly to the substations with the same name. These substations are only separated by a transmission line, and the lines passing through VIL and TRA connect respectively with them. Records at VIL have been especially noisy, as reflected in Table 1. Moreover, we can detect when a power line is switched off from the grid (as at SAN for the 23–26 April 2021 event), because the magnetic records are virtually the same in both the magnetometer under the line and the reference one, with a clear reduction of the noise in the former.

We have only been able to pick up GIC signals during a few events, corresponding to low to moderate magnetic activity during the last months. However, the available data shows that the performances evaluated by the  $P'$  parameter at the power line passing through TRA are lower than those obtained when comparing the modeled GIC with the measured ones at the neutral of a transformer linked to the same power line during different geomagnetic storms from September 2011 to June 2012 (Torta et al., 2017). In those occasions,  $P'$  ranged from 0.14 to 0.45 while in the present study we mostly find negative values. The better performance of the former may be partially explained by the larger geomagnetic activity on that period, with maximum  $K_p$  values ranging from 5 to 8; indeed, larger activity levels are expected to produce better performances, since the GIC signal is more clearly above the intrinsic noise threshold.  $P'$  is the recommended score to evaluate how skillful a model is at predicting the observations. Its value for consistent GIC models generally does not go above 0.6–0.7, because there are considerable uncertainties concerning (a) the MT impedance tensor variability across the different power grid terrains, (b) the line, transformer winding and grounding resistances, and (c) the power grid status, with frequent switching on and off and renewals of power lines and transformers.

## 6. Discussion and Conclusions

We have given thorough details of the procedure we used to validate the modeling of GIC by measuring the magnetic effect of the induced currents in four 400 kV lines of the Spanish power grid. The procedure was initially tested by a pilot DMM deployment monitoring a power line that runs SW-NE, parallel to the Mediterranean coast, approximately 12 km away from Ebre Geomagnetic Observatory. The precariousness of the first installation and, probably, the inadequacy of the magnetometers initially used for this purpose, prevented obtaining satisfactory results. The lessons learned during those pilot tests and those from other subsequent preliminary sites were used to start the operational measurements during the summer of 2020.

The performance parameter of the modeled versus DMM-derived GIC found at TRA station is lower than the one found when the measurements were carried out in the neutral of a transformer linked to the same transmission line, arguably because of the higher signal-to-noise ratio of the GIC data associated with the events analyzed during the direct method, among other intrinsic advantages of this technique over the DMM.

Testing during our first deployments coincided with a period of extremely low geomagnetic activity at the end of the Solar cycle 24. This low level of activity continued through the beginning of Solar cycle 25, coinciding with our reported case studies, thus limiting the possibilities of having a clean signal. Only during the last few months magnetic activity began to increase, giving hope of better signals in the future.

Instead of relying on geomagnetic activity indices, we took the time derivative of the horizontal geomagnetic field at EBR geomagnetic observatory as a proxy for the GIC activity level. The few events of moderate activity hardly allow us to detect differences of a dozen nanoteslas between magnetometers mag1 and mag2, which translate into GIC signals of a few amps at most, though the signal barely exceeds the noise level for most of the time. Following the procedure that we have established would certainly have resulted in a more remarkable signal-to-noise ratio at higher latitudes than Spain.

Electromagnetic noise is thus a serious problem inherent in the DMM. Some of it is man-made and can be partially prevented by proper selection of the measurement site. Another part is introduced by the measurement system itself and its peripherals (e.g., data transmission, solar panel electronics and cabling). A thoughtful choice of the features of the magnetometer to be used is essential. An important part of the noise flows in the power line and is suspected to be related to power grid switching or voltage transients originating from high-power demanding. This type of noise leaks into the magnetometers and is difficult, if not impossible, to anticipate when planning a temporary DMM station. A short test period is advisable to check for the existence of noise prior to the definitive

installation. An assessment of the uncertainty associated with the intrinsic (i.e., excluding the ambient noise) process of GIC estimation shows that our instrumentation and procedures are adequate, with absolute uncertainties of the order of 0.06 A and relative uncertainties below 3% in any case. The ambient noise depends on each individual power line and DMM site and can introduce spurious signals ranging between several hundredths and several tenths of an amp in the finally reported GIC.

In any case, since it is not possible to instrument all transformers or all power lines in a network, the ultimate goal of GIC measurement is the local validation of models that more or less efficiently provide GIC estimates for all power transmission lines, nodes and transformers. Our first results with the DMM reveal good correlations ( $\rho$ ) with the GIC modeled at TRA, SAN, VIL, and especially at LUC, which denotes that we are modeling successfully the waveform of the GIC. Because the lithosphere acts as a filter of the incoming electromagnetic wave, this suggests that the 3D lithospheric resistivity model works quite well in areas where it enjoyed a dense distribution of MT data to be inverted (see Figure 1 from Torta et al., 2021). However, the lack of agreement in the GIC amplitude in some of the monitored power lines, as reflected by the  $P'$  skill score, indicates the possible existence of errors in some assumed values for the resistances of the network elements. Ignoring the network below 220 kV in the vicinity of those lines might also have been too strong an assumption.

## Data Availability Statement

The geomagnetic observatory data were obtained from [www.intermagnet.org](http://www.intermagnet.org). In addition, EBR geomagnetic data are available from <http://www.obsebre.es/en/en-om-data-catalogs-ebre>. The magnetometer data to derive the GIC are available in this in-text data citation reference: Marsal et al. (2021) (under license CC-BY-ND).

## Acknowledgments

This research has been supported by Spanish projects CGL2017-82169-C2-1-R, CGL2017-82169-C2-2-R funded by Ministerio de Ciencia, Innovación y Universidades, and PID2020-113135RB-C32, funded by Ministerio de Ciencia e Innovación. It was also partially funded by "la Caixa" Foundation. We are grateful to the owners of the lands where we have deployed our instruments for lending us a space free of charge. We are also grateful to two anonymous reviewers for their useful comments, which helped to improve the manuscript. Some of the results presented in this paper rely on data collected at geomagnetic observatories; we thank the national institutes that support them, and INTERMAGNET for promoting high standards of geomagnetic observatory practice.

## References

- Bailey, R. L., Halbedl, T. S., Schattauer, I., Achleitner, G., & Leonhardt, R. (2018). Validating GIC models with measurements in Austria: Evaluation of accuracy and sensitivity to input parameters. *Space Weather*, 16(7), 887–902. <https://doi.org/10.1029/2018SW001842>
- Blake, S. P., Gallagher, P. T., Campaña, J., Hogg, C., Beggan, C. D., Thomson, A. W. P., et al. (2018). A detailed model of the Irish high voltage power network for simulating GICs. *Space Weather*, 16, 1–1783. <https://doi.org/10.1029/2018SW001926>
- Boteler, D. H., & Pirjola, R. J. (2017). Modeling geomagnetically induced currents. *Space Weather*, 15(1), 258–276. <https://doi.org/10.1002/2016SW001499>
- Campbell, W. H. (1978). Induction of auroral zone electric currents within the Alaska pipeline. *Pure and Applied Geophysics*, 116(6), 1143–1173. <https://doi.org/10.1007/BF00874677>
- Campbell, W. H. (1980). Observation of electric currents in the Alaska oil pipeline resulting from auroral electrojet current sources. *Geophysical Journal of the Royal Astronomical Society*, 61(2), 437–449. <https://doi.org/10.1111/j.1365-246X.1980.tb04325.x>
- Hübner, J., Beggan, C. D., Richardson, G. S., Martyn, T., & Thomson, A. W. P. (2020). Differential magnetometer measurements of geomagnetically induced currents in a complex high voltage network. *Space Weather*, 18(4), e2019SW002421. <https://doi.org/10.1029/2019SW002421>
- Ingham, M., Rodger, C. J., Divett, T., Dalzell, M., & Petersen, T. (2017). *Assessment of GIC based on transfer function analysis* (pp. 1–13). <https://doi.org/10.1002/2017SW001707>
- Korepanov, V., Berkman, R., Rakhlin, Y., Prystai, K. A., Marussenkov, A., Afanassenko, A., & Afanassenko, M. (2001). Advanced field magnetometers comparative study. *Measurement*, 29, 137–146. [https://doi.org/10.1016/s0263-2241\(00\)00034-8](https://doi.org/10.1016/s0263-2241(00)00034-8)
- Lehtinen, M., & Pirjola, R. J. (1985). Currents produced in earthed conductor networks by geomagnetically-induced electric fields. *Annales Geophysicae*, 3(4), 479–484.
- Love, J. J., Rigler, E. J., Kelbert, A., Finn, C. A., Bedrosian, P. A., & Balch, C. C. (2018). *On the feasibility of real-time mapping of the geoelectric field across North America*: Open-File Report. <https://doi.org/10.3133/ofr20181043>
- Mac Manus, D. H., Rodger, C. J., Dalzell, M., Thomson, A. W. P., Clilverd, M. A., Petersen, T., et al. (2017). Long-term geomagnetically induced current observations in New Zealand: Earth return corrections and geomagnetic field driver. *Space Weather*, 15(8), 1020–1038. <https://doi.org/10.1002/2017SW001635>
- Mäkinen, T. (1993). *Geomagnetically induced currents in the Finnish power transmission system*: Finnish Meteorological Institute.
- Marsal, S., & Torta, J. M. (2019). Quantifying the performance of geomagnetically induced current models. *Space Weather*, 17(7), 941–949. <https://doi.org/10.1029/2019sw002208>
- Marsal, S., Torta, J. M., Curto, J. J., Canillas-Pérez, V., Cid, O., Ibañez, M., & Marcuello, A. (2021). Validating GIC modelling in the Spanish power transmission grid by differential magnetometry [Dataset]. DIGITAL.CSIC. <https://doi.org/10.20350/digitalCSIC/14004>
- Marshall, R. A., Kelly, A., Van Der Walt, T., Honecker, A., Ong, C., Mikkelsen, D., et al. (2017). Modeling geomagnetic induced currents in Australian power networks. *Space Weather*, 15(7), 895–916. <https://doi.org/10.1002/2017SW001613>
- Matandirotya, E., Cilliers, P. J., Van Zyl, R. R., Oyedokun, D. T., & de Villiers, J. (2016). Differential magnetometer method applied to measurement of geomagnetically induced currents in Southern African power networks. *Space Weather*, 14(3), 221–232. <https://doi.org/10.1002/2015SW001289>
- Schachinger, P., Albert, D., & Renner, H. (2021). Geomagnetically induced currents: A measurement based inverse determination of earth impedances, 56th International Universities Power Engineering Conference (UPEC), 1-5. <https://doi.org/10.1109/UPEC50034.2021.9548157>
- Torta, J. M., Marcuello, A., Campaña, J., Marsal, S., Queralt, P., & Ledo, J. (2017). Improving the modeling of geomagnetically induced currents in Spain. *Space Weather*, 15(5), 691–703. <https://doi.org/10.1002/2017SW001628>
- Torta, J. M., Marsal, S., Ledo, J., Queralt, P., Canillas-Pérez, V., Piña-Varas, P., et al. (2021). New detailed modelling of GICs in the Spanish power transmission grid. *Space Weather*, 19(9), e2021SW002805. <https://doi.org/10.1029/2021SW002805>



- Torta, J. M., Marsal, S., & Quintana, M. (2014). Assessing the hazard from geomagnetically induced currents to the entire high-voltage power network in Spain. *Earth, Planets and Space*, *66*(1), 1–17. <https://doi.org/10.1186/1880-5981-66-87>
- Torta, J. M., Serrano, L., Regué, J. R., Sánchez, A. M., & Roldán, E. (2012). Geomagnetically induced currents in a power grid of northeastern Spain. *Space Weather*, *10*(6), S06002. <https://doi.org/10.1029/2012SW000793>
- Trivedi, N. B., Vitorello, Í., Kabata, W., Dutra, S. L., Padilha, A. L., Mauricio, S. B., et al. (2007). Geomagnetically induced currents in an electric power transmission system at low latitudes in Brazil: A case study. *Space Weather*, *5*, S04004. <https://doi.org/10.1029/2006SW000282>